 DOI: 10.1002/masy.201050401

Long-Range Processing Correlation and Morphological Fractality of Compatibilized Blends of PS/ HDPE/ SEBS Block Copolymer

Želimir Jelčić,[*1] *Nina Vranješ,*[2] *Vesna Rek*[2]

Summary: Processing and compatibilization effects of a commercially available styrene/ ethylene-butylene/ styrene (SEBS) compatibilizer on the morphological structure, rheological and mechanical properties of blends of polystyrene (PS) and high density polyethylene (HDPE) were investigated. The rheological behaviour of the blends melt during processing was followed by measuring torque; extrusion capacity output and melts back-pressure in a twin screw extruder. The processing parameters were decreased with the HDPE content. The results show that SEBS compatibilizer can yield compatibilization by substantially reducing torque and increasing the back-pressure. However, the Hurst indices of melt processing parameters are increased with compatibilization. Near-infrared spectra had been described by the Hurst index H_{NIR} which is then related to HDPE content in the blends. The correlation between the blend compositions, morphological structure, mechanical and rheological properties and processing parameters was established and discussed on base of correlation with the fractal indices obtained from the SEM microphotographs of PS/ HDPE/SEBS blends.

Keywords: fractal; Hurst index; mechanical properties; morphology; processing; PS/HDPE/ SEBS blends; rheological properties; structure

Introduction

Polystyrene (PS) and polyethylene (PE) are two of the most widely used plastics in the world. Polystyrene is incompatible with polyethylene. The problem of their incompatibility may be resolved by a compatibilizer.[1] Compatibilization by styrene/ ethylene-butylene/ styrene (SEBS) compatibilizer promotes the formation of the new morphological structure in PS/ PE blends, which allow more equal sharing of imposed stresses and might therefore, improve the mechanical and rheological properties of the blends, significant for the users. Decrease of stiffness and increase creep value of PS is possible by adding PE whose high creep value can be modified by PS.[2,3,4] The effect of compatibilization on the morphology of the PS/PE blends has been extensively studied.[5,6] Phase separation of polymer blends can create spheres, rods, cubes, and lamellae depending on the different environments where the component polymers are located. Each of these structures varies its morphology and function with slight changes in chemical structure and composition of polymers in polymer blend.[7,8] This phase separated structures can create higher-order fractal structures. It has been established that the micro-domain structure in phase separated blends changes in a much more complicated fashion than in neat polymers. These fractal structures determine the creep behaviour

[1] PLIVA Croatia Ltd., TAPI R&D, Prilaz baruna Filipovića 29, HR10000 Zagreb, Croatia
Fax (+385)1 3721827;
E-mail: zelimir.jelcic@pliva.hr
[2] Faculty of Chemical Engineering and Technology, University of Zagreb, Marulićev trg 19, HR10000 Zagreb, Croatia

and creep modulus. The mechanical properties, rheological properties in blends processing as well as creep behaviour of blends extruded and moulded samples were studied to obtain the correlation between blends composition, morphological structure and mentioned properties.

Estimation of the Hurst Parameter of Processing Parameters Dependent Time Series

The subject of self-similarity and the estimation of statistical parameters of time series in the presence of long-range dependence are becoming more and more common in several fields of science. Recent evidence suggests that processing signals under steady conditions may have a fractal temporal structure. We investigate the possibility that timed series generated by certain processing control systems may be members of a special class of complex fractal processes, which require an exponent to characterize their scaling properties. Processing signals are generated by complex self-regulating systems that process inputs with a broad range of characteristics. Many processing time series are extremely inhomogeneous and non-stationary, fluctuating in an irregular and complex manner. Fractal signals are homogeneous in the sense that they have the same scaling properties throughout the entire signal. Therefore, fractal signals can be indexed by a single global exponent called Hurst's exponent, H.[9] The fractal signals exhibit long-range persistence dependence, which is also called the Joseph effect, referring to the ''seven fat years and seven lean years'' in the Biblical story of Joseph. The predominant way to quantify long-range dependence is the value of the Hurst exponent. However, a time series can be tested for correlation in many different ways.[10] Therefore, different methods that can be used to estimate the Hurst exponent often produce conflicting estimates. The following Hurst exponent estimators are evaluated [11]: *Absolute Value method*, where an aggregated series $X(m)$ is defined, using different block sizes m. The log-log plot of the aggregation level versus the absolute first moment of the aggregated series $X(m)$ should be a straight line with slope of H-1, if the data are long-range dependent; *Variance method*, where the log-log plot of the sample variance versus the aggregation level must be a straight line with slope β greater than -1; the Hurst index is then given by $H = 1\text{-}\beta/2$; *Periodogram method:* The slope of the logarithm of the spectral density of a time series plotted versus the logarithm of the frequencies provides an estimate of H; *Whittle estimator*: The method is based on the minimization of a likelihood function, which is applied to the periodogram of the time series; *Variance of Residuals*: A log-log plot of the aggregation level versus the average of the variance of the residuals of the series should be a straight line with slope of H/2; *Abry-Veitch estimator*[12]: A least-squares fit on the average of the squares of the wavelet coefficients at different scales is an estimate of the Hurst exponent; *R/S method*: A log-log plot of the R/S statistic versus the number of points of the aggregated series should be a straight line with the slope being an estimation of the Hurst exponent. The R/S statistic is a well-known and accepted technique for estimating the Hurst parameter (Autosignal Windows version 1.6, AISN Software Inc.).[13] The objective of the R/S analysis of processing signal record is to infer the degree of self-similarity by Hurst's index, H for the self-similar process that presumably generates the record under consideration. The Hurst exponent measures the fractal dimension of a processing data series. A Hurst exponent of 0.5 indicates no long-term memory effect. The signal will then tend to make long excursions upwards or downwards. As H goes towards 1, the signal becomes more and more monotonous. Higher values of Hurst's exponent indicate an increasing presence of long-term memory effect. The closer the value of the Hurst index H is to 1, the more slowly the variance decays as scale increases, and the process is said to be more

''*bursty*''. Statistical self-similar means that the statistical properties for the entire data set are same for sub-sections of the data set (the two halves of the data set have the same statistical properties as the entire data set). This is applied to estimate the Hurst exponent, where the rescaled range is estimated over sections of different size. The Hurst exponent is also directly related to the fractal dimension, D, by D = 2 - H. However, to avoid confusion, we would use the Hurst index term for the 1D objects (time series and spectra), and fractal dimension for the 2D objects (images).

Fractal Analysis

Fractal geometry is used for the quantification of a fracture surface roughness. It has been shown that the fractal-based methods appear to be suitable for describing structures and processes in polymer blend systems.[14] This is because the morphology of fracture surface exhibits a fractal nature, i.e., it has details at many scales and also a part of a polymer blends fracture surface at a large scale is similar to a part of the surface at a small scale. The fractal concept was first proposed by Mandelbrot,[15] who introduced dimensions between the conventional Euclidean dimensions of 1, 2, and 3 to describe structures that are not Euclidean lines, surfaces or solids. The fractal dimension indicates the degree to which an image deviates from smoothness and regularity. For example, a fractal dimension from 1 to 2 describes the area-filling capacity of a convoluted line and a fractal dimension from 2 to 3 describes the volume filling capacity of a highly rugged surface.[16,17,18] A characteristic of fractal objects is ''self-similarity'', the attribute of having the same appearance at all magnifications. However, real materials or ''natural fractals'' are self-similar only over a limited range of scales.[16,19] Although polymer blends fracture surface structures may exhibit different characteristics; for example, irregular-chunky, smooth-flaky, fibrous, sponge, terrace and granular, they possess a common fractal property called ''piecewise self-transformability'', i.e., they contain transformed copies of parts of themselves. This fractal property of ''self-transformability'' is illustrated by several regions on the fracture surface image that is similar in different scales. The SEM images are projected images of fractured polymer blends surfaces, and they do not represent three-dimensional 3-D elevation data of the surfaces. This 3-D surface data can be obtained from range images, i.e., images produced by encoding the 3-D elevation data into different gray-scale levels.[20] SEM images of polymer blends fracture surfaces were converted to binary maps (object pixels = black, non-object (void) pixels = white).[21] The images were binarized by an automatic thresholding (at 128 pixel intensity thresholds), although such procedure tended to give hollow primary particles due to its high sensitivity to the particle boundaries. From the binary images three 2D parameters were retrieved: the ''classical'' box counting D_{BBW}, interface D_{BW} and ''void'' D_{WBW} fractal indices of the projected surface area. Fractal indices of SEM images are calculated by a freeware texture correlation programme (HarFA).[22] The effects of resolution on the projected surface area, fractal dimension and other shape parameters derived from 2D images were also investigated. The magnification and resolution of the images are important factors because narrow morphological features of aggregates could yield a biased result when they are not adequately resolved.[23] The scatter in fractal dimensions is due to both the influence of resolution and the real structural variations of objects.[24] The changes in fractal indices with magnification are due to the failure to detect intricate features on the aggregates, and due to the underestimation of the primary particle circumference at a coarse resolution.[25] The generalized dimension D_q of a process is defined as (IQM 1.16 by H. Ahammer):

$$D_q = \frac{1}{1-q} \lim_{T \to 0} \left[\frac{\log(\sum Z_k^q)}{\log(T)} \right]$$

where data segment of length L is divided into intervals of length T, with Z_k representing the number of points in the k-th interval, and the sum extends over all non-empty intervals. Particular cases are the capacity or box counting dimension D_0, the information dimension D_1, and the correlation dimension D_2. The Higuchi's dimension D_h is a length-based fractal of a curve.[26,27] Among the various fractal dimension methods, the Higuchi fractal method is well suited for studying signal fluctuation in one dimension. The SEM image of non-compatibilized and compatibilized blends is transformed into 1-D signals (''landscapes'') that are subsequently analysed to determine roughness of a broken surface of a specimen. This dimension is more appropriate for stochastic, rather than deterministic, series with continuous curves giving a value $D_h = 1$, and self-similar stochastic curves giving a value $D_h = 1.5$, which is the value expected for Brownian motion. Chaotic time series acts as a plane-filling curve. Whether a data series is truly a fractal object when fractal dimension value is extractable can still be a debatable issue for the sake of finding the truth. The pragmatic approach was taken in that when the Higuchi fractal algorithm extracts a fractal dimension with a good coefficient of determination R^2 value of the log-log graph, then the image can be treated as a fractal object as far as application is concerned.

Separation of Images into Waviness and Roughness Images

Surface texture is the combination of fairly short wavelength deviations of a surface from the nominal surface. Texture includes roughness and waviness, so that the SEM images can be separated into ''waviness'' and ''roughness'' images by use of a large Gaussian Filter kernel. This might often be desirable when measuring roughness within specific wavelength intervals. The smoothening effect of the large filter creates the Waviness image where only the long waves are seen. Waviness includes the more widely spaced (longer wavelength) deviations of a surface from its nominal shape. The difference between the original image and the Waviness image is the Roughness image where only the short waves are seen. Roughness includes the finest (shortest wavelength) irregularities of a surface. Roughness generally results from a particular production process or material condition. It is often desirable to measure the roughness on the roughness image rather than the raw image, which can be dominated by the long waves. The ''waviness'' was separated from the ''roughness'' in the SEM images by an ImageJ add-in.[28]

Topological Analysis by Thinning

The thinning (or edge detection) function generates a minimally connected line that is equidistant from the boundaries. A thinning algorithm was applied to the binary image to create an image containing only the image ''skeleton'', representing the pixels in each pixel group that are essential for communicating the shape of the given pixel group. The thinning relates to the minimal structure of the image, informing hierarchies, branches and angles among branches of this image. Thinning of the raster image to single pixel width lines was performed as a multi-class segmentation in a gray level domain according to the Zhang and Suen[29] algorithm in order to make the complex nature of the matrix observable. The binary skeleton was further processed to identify fractal indices of branching points (the nodes where branches meet) and internal holes (the empty regions). Hence, we are dealing with length fractals, and the obtained fractal dimension D_{ZS} of Zhang and Suen thinned SEM images is expected to show values of $1 < D_{ZS} < 2$. The Zhang-Suen thinning method has been here applied also for the SEM images of blends, and further the fractal dimension was estimated. Thus, thinned SEM images show fractal properties only in a statistical sense and are limited to a certain range of scale.

Two-Dimensional Correlation Spectroscopy (2D-COS)

The basic concept of two-dimensional (2D) correlation analysis may be regarded as a form of manipulation and comparison of two sets, representing the time, temperature, spatial, concentrations, or pressure-dependent signals/ spectra, measured at two independent spectral variables, such as wavenumbers.[30] The pair-wise comparison of two sets generates a correlation intensity defined by the given form of a correlation function. The array of correlation intensities plotted as a function of two independent spectral variables then becomes a 2D correlation spectrum.[31,32,33] The synchronous spectrum gives information about spectral features that change in phase (i.e., occur at the same time). The synchronous spectrum is symmetric about the diagonal and resembles a graphical presentation of a multivariate covariance calculation. The asynchronous spectrum resembles the synchronous spectrum; however, it indicates covariance that occurred 90° out-of-phase (i.e., measure changes in spectral features that vary independently). In addition, the arc tangent of the ratio of the peak intensities of the asynchronous and synchronous spectra gives the phase angle between the two events. The generalized 2D-COS formalism has been applied to conformational changes and specific interactions in polymer blends.[34,35,36,37] In this paper, we explore a new application of generalized 2D-COS to the analysis of NIR spectra of a compatibilized heterogeneous polymer blend sample with components of continuously varying concentration.

Experimental Part

Bi- and tri-component blends were prepared from general purpose polystyrene, PS, Dow Styrene 678E GPPS, Dow Plastics; MFR 10.5 g/10 min (conditions 200 °C, 5 kg); injection grade high density polyethylene, HDPE, Lupolen 5031L, Basell Polyolefins Italia; density 0.952 g/cm^3, MFR 6.5 g/10 min (190 °C, 2.16 kg) and SEBS Kraton G1650, Shell Co., as compatibilizer with a content of PS 29% wt. The samples of neat polymers and blends were prepared by Haake Record 90 twin extruder with intensive mixing profile, Haake TW 100, with the following temperatures in zone 180/ 195/ 210/ 210 °C. Torque and melt back-pressure during processing in the twin screw extruder were recorded at one and six seconds' interval, respectively. The specimens were obtained by compression injection moulding at 230 °C by a laboratory injectometer (Zwick, mould temperature 40 °C, and the injection rate 200 mm/s). The scanning electron microscope (SEM) JEOL JSM5800, was used to investigate the morphology of samples after the specimens were broken under liquid nitrogen atmosphere. Near-infrared spectra were obtained by Bruker MPA instrument, in the range of 12500-3600 cm^{-1}, averaging 32 scans per spectra at the resolution of 8 cm^{-1}. Tensile strength and elongation at break were measured according to standards ISO 527-1:1993 and ISO 527-2: 1993 by Instron 1185 instrument. Notched Izod impact strength was measured according to ISO 180: 1993.

Results and Discussion

Processing Parameters

Torque values increase with increasing PS and HDPE content in the PS/ HDPE/ SEBS blends. However, torque by extrusion of the PS/ HDPEP/ SEBS blends is not changed drastically. The reduced ratio (Torque/ Output) decreases by increasing HDPE content in the PS/ HDPE/ SEBS blends ($|R| = 0.979$; $F_{signif}(2,9) = 1.3 \times 10^{-9}$):

$$(\text{Torque}/\text{Output})\,(\text{Nm} \times \text{h}/\text{kg}) = 6.98 - 0.0292 \times \text{HDPE}(\%)$$

The reduced back-pressure decreases by increasing PS or HDPE content in

Table 1.
Hurst indices H_{torque} from torque, and H_{back} from back-pressure processing time series.

PS (phr)	HDPE (phr)	SEBS (phr)	Hurst index					
			H_{torque}	St. dev.	R^2	H_{back}	St. dev.	R^2
0	100	0	0.7997	0.0094	0.921	0.6837	0.0064	0.966
20	80	5	0.8776	0.0049	0.994	0.7841	0.0040	0.992
20	80	7	0.8728	0.0053	0.979	0.7060	0.0094	0.927
40	60	0	0.8080	0.0093	0.998	0.6054	0.0031	0.986
40	60	5	0.8776	0.0040	0.998	0.8354	0.0050	0.999
40	60	7	0.8296	0.0099	0.922	0.7146	0.0103	0.943
60	40	5	0.7952	0.0012	0.994	0.7055	0.0059	0.967
60	40	7	0.8054	0.0016	0.992	0.7166	0.0479	0.972
80	20	0	0.8062	0.0040	0.958	0.6952	0.0046	0.976
80	20	5	0.8375	0.0014	0.999	0.7283	0.0036	0.981
80	20	7	0.8203	0.0030	0.974	0.6827	0.0028	0.989
100	0	0	0.8045	0.0042	0.944	0.7837	0.0036	0.985

blends ($|R| = 0.801$; $F_{signif}(2,11) = 0.003$):

$$(\text{back} - \text{pressure/Output})\,(\text{bar} \times \text{h/kg}) = 51.89 - 0.354 \times \text{PS(wt.\%)} - 0.416 \times \text{HDPE(wt.\%)}$$

The observed outlier corresponds to the pure HDPE processing parameters. The amount of SEBS does not influence statistically significant the reduced processing parameters. Hurst's indices H_{torque} from torque and H_{back} from back-pressure processing time series (by (R/S) method, Table 1) non-linearly depend on the blend composition (Figure 1). The largest Hurst index values are observed for the PS/HDPE/5 phr SEBS blends. The R/S statistic has given the best estimation of the Hurst parameter by composition.

Morphological Structure

SEM images of the PS/HDPE blends reveal two phase morphology of the well-organized ''islands'' of the polymer blends components HDPE or PS particles in the PS or HDPE matrix as well as the presence of cavities[38] (Figure 2). PS is much more brittle than most polymers.[39] Therefore, smaller PS islands in the HDPE matrix are desirable. Poor interfacial adhesion between the phases can be observed.[40] The microstructure of the PS/HDPE blends is changed by adding SEBS. The SEM micrographs show a reduction in particle size of the dispersed phase in the blends with compatibilizer – what suggests a reduction in interfacial tension between HDPE and PS. Blends formed far from equilibrium (non-compatibilized blends) have higher fractal dimensions in comparison

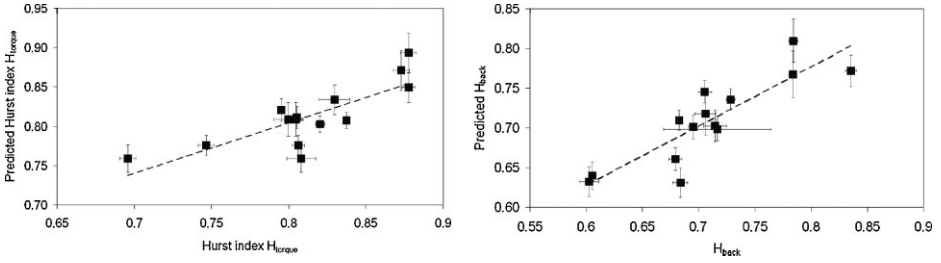

Figure 1.
Hurst index H_{torque} (left) and H_{back} (right) predicted by blend composition: $H_{torque} = 0.809 - 2.06 \times 10^{-5} \times PS(\%) \times HDPE(\%) + 0.00066 \times HDPE(\%) \times SEBS(\%) - 7.237 \times 10^{-5} \times HDPE(\%) \times (SEBS(\%))^2$; $|R| = 0.803$; $F_{signif}(3,10) = 0.01$(left); $H_{back} = 0.631 - 0.0001767 \times HDPE(\%) \times (SEBS(\%)^2 + 1.363 \times 10^{-7} \times (PS(\%))^3 + 0.00133 \times HDPE(\%) \times SEBS(\%)$; $|R| = 0.865$; $F_{signif}(3,10) = 0.002$) (right).

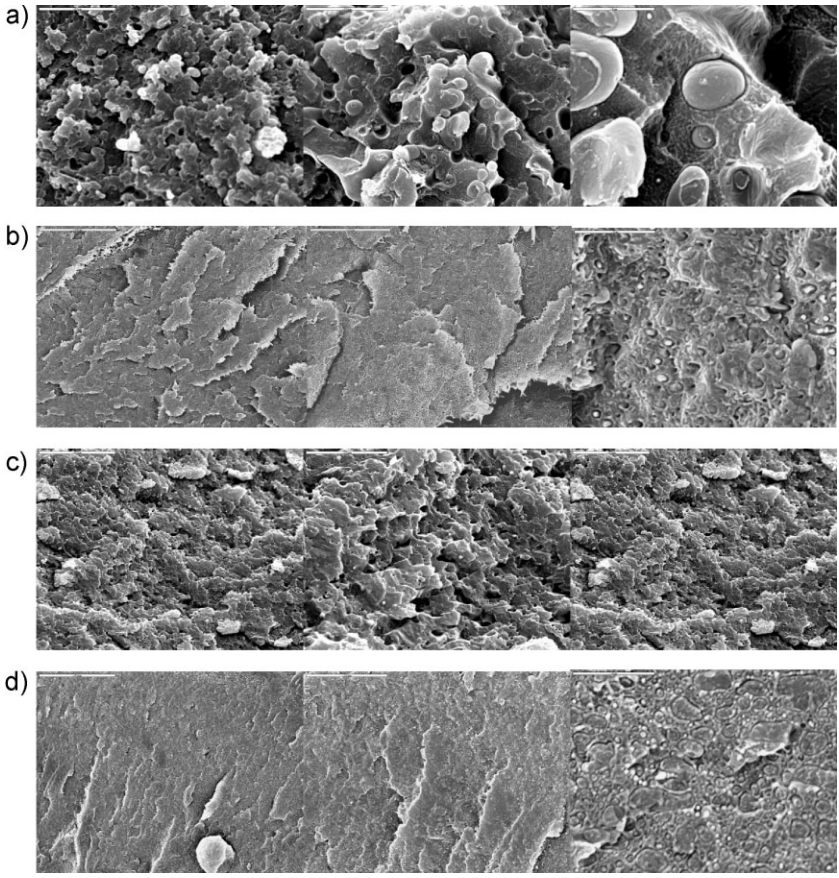

Figure 2.
SEM microphotographs of the fracture surface of PS/ HDPE/ SEBS blends: 40/60/0 (a), 40/60/7 (b), 80/20/0 (c) and 80/20/7 (d) at various magnifications; image area: 22716 μm^2 (left), 3225 μm^2 (middle) and 198.8 μm^2 (right).

to blends formed by compatibilization (Figure 3, left). This is observed empirically as a transition from swallow-tail and dendrite shapes to objects having a more compact density distribution. Fractal indices derived by the box counting method are given as a function of polymer blends components and the magnification of SEM images (Table 2).

The fractal indices derived by the wavelet method have larger error range and the regression is not as convincing as that with the fractal indices derived from the ''original'' SEM images or the thinned ones. The Higuchi's dimension D_h of blend SEM images depended on the SEBS content (and the SEM image size) (Figure 3, right). Higuchi's dimension values are larger than 1.5 indicating self-similar stochastic to plane-filling curves as representation of SEM images. Morphological ''classical'' box counting fractal index D_{BBW} and the processing Hurst index H_{torque} from torque measurements are linearly correlated ($R^2 = 0.633$). Even better correlation is observed for correlation of D_{BBW} with the Hurst index, H_{back}, from back-pressure measurements ($R^2 = 0.944$) (Figure 5, left).

Fractal indices derived from the SEM images thinned by the Zhang-Suen method can be described by the magnification (scale bar value) and SEBS content (Table 3, Figure 4 c, d). The morphological

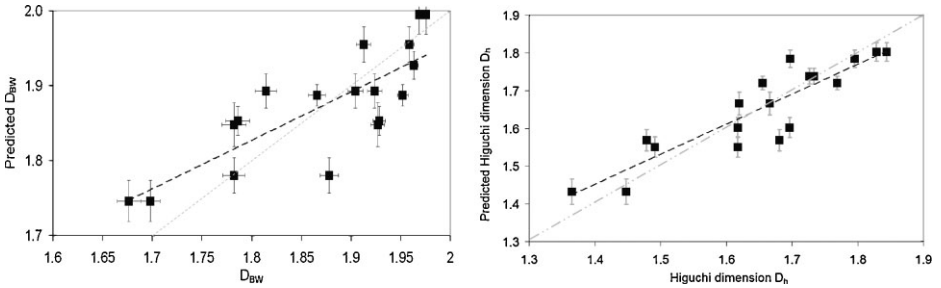

Figure 3.
Predicted interface fractal index D_{BW} (Table 2) (left), and the Higuchi fractal dimension D_h (right) by SEBS content in blends; $D_h = 1.570 + 0.03576 \times$SEBS(%) $-6.05 \times 10^{-6} \times$image area($\mu m^2$), $|R| = 0.893$; $F_{signif}(2,15) = 6.4 \times 10^{-6}$ (right).

Table 2.
Regression coefficients of fractal indices of SEM images; $D = a_0 + a_1 \times$SEBS(%) $+a_2 \times$HDPE(%) $+a_3 \times$scale bar(μm); correlation coefficient R; significance F_{signif}(k,n-k-1), where n is the number of data points, k number of model parameters.

Fractal index	Regression coefficients				R	F_{signif}(k,n-k-1)
	a_0	a_1	a_2	a_3		
D_{BW}	1.734	0.02248	–	0.00227	0.806	0.0002 (2,16)
D_{BBW}	1.956	0.00285	−0.000289	0.000614	0.805	0.001 (3,15)
D_{WBW}	1.867	0.01177	–	–	0.609	0.005 (1,17)

Table 3.
Regression coefficients of fractal indices of SEM images thinned by the Zhang-Suen method; $D = a_0 + a_1 \times$SEBS(%) $+ a_2 \times$scale bar(μm); correlation coefficient R; significance F_{signif}(k,n-k-1), where (n-k-1) is the model degree of freedom, n number of data points, k number of model parameters.

Fractal index	Regression coefficients			R	F_{signif}(2,16)
	a_0	a_1	a_2		
$D_{BW,ZS}$	1.762	0.01786	0.00225	0.842	5.15×10^{-5}
$D_{BBW,ZS}$	2	4.11×10^{-5}	−0.000227	0.846	4.18×10^{-5}
$D_{WBW,ZS}$	1.722	0.01843	0.00239	0.849	3.78×10^{-5}

"classical" box counting fractal index D_{BBW} (from the Zhang-Suen thinned SEM images) and the processing Hurst index H_{torque} from torque measurements are well linearly correlated ($R^2 = 0.859$) (Figure 5, right). Alike is observed for correlation with the Hurst index H_{back} from back-pressure measurements ($R^2 = 0.775$).

Generalized fractal dimensions D_q revealed different sensitivity of non-compatibilized and compatibilized blends on SEM magnifications. Non-compatibilized PS/HDPE 80/20 blend at negative q-parameters differ at large in fractal dimension D_q. By compatibilization, fractal dimensions D_q are almost same in the whole range of q-parameters (Figure 7).

Near-Infrared Spectra

Near-infrared (NIR) spectra have been measured for polystyrene (PS), high density polyethylene (HDPE) and their blends without and with 5 phr and 7 phr of SEBS of PS/HDPE different compositions. As the content of HDPE increases, the intensity of a CH methylene peak at 1540 nm appears. Also, the intensity of peaks at 1217 nm and at 1732 nm increases with the increase of HDPE content. These two peaks are due to the second and first overtones of C-H methylene stretching in polyethylene.

NIR spectra of non-compatibilized and compatibilized PS/HDPE blends differ in intensity sensitivity to composition (Figure 8). The compatibilized blends have

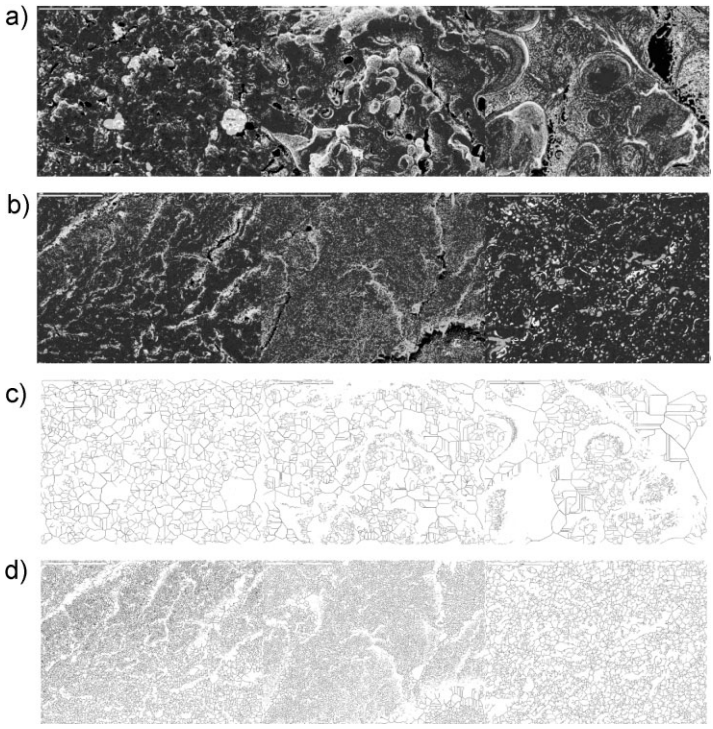

Figure 4.
"Waviness" (a, b) and by Zhang-Suen algorithm thinned (c, d) SEM microphotographs of the fracture surface of PS/ HDPE/ SEBS blends: 80/20/0 (a, c) and 80/20/7 (b, d) at image area of 22716 μm^2 (left), 3225 μm^2 (middle) and 199 μm^2 (right).

almost identical NIR spectra, and the non-compatibilized are sensitive to the composition. Composition-dependent spectral variations of the blends have been analysed by generalized two-dimensional (2D) correlation spectroscopy to study the conformational changes and specific interactions in the blends. The NIR spectra have been divided into two sets for the 2D correlation: the set of blends without compatibilizer (no SEBS), and the set of compatibilized blends with 5 phr and 7 phr of SEBS. The 2D synchronous correlation analysis discriminates between the bands of PS and those of HDPE and detects bands that are not readily identifiable in the one-dimensional

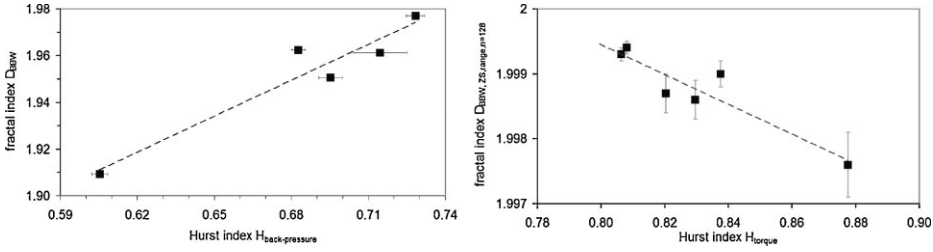

Figure 5.
Correlation of "classical" box counting fractal index D_{BBW} (at threshold n = 128) and the back-pressure based Hurst index H_{back} for PS/HDPE/SEBS blends (left); Correlation of Zhang-Suen thinned SEM images fractal index $D_{BBW,ZS}$ and the torque based Hurst index H_{torque} for PS/HDPE/SEBS blends (right).

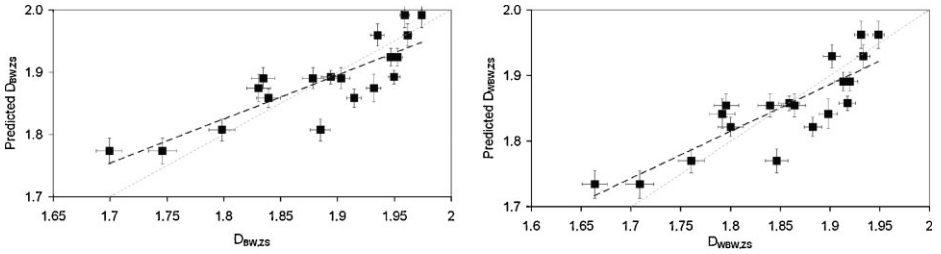

Figure 6.
Correlation of predicted (by linear function of SEBS content and scale bar value) and from thinned SEM images by Zhang-Suen method derived interface fractal index $D_{BW,ZS}$ (left) and ''void'' fractal index $D_{WBW,ZS}$ (right) (see Table 3).

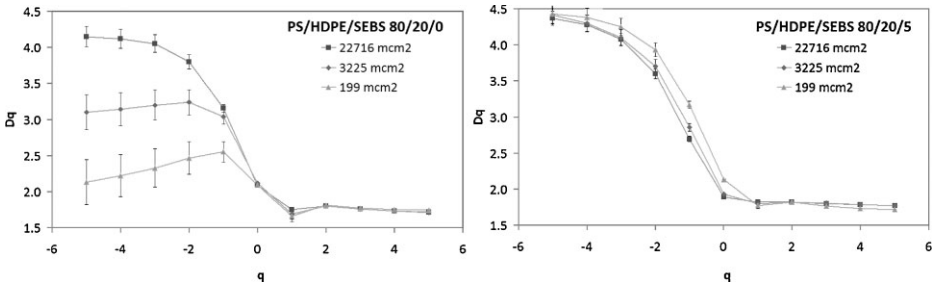

Figure 7.
Generalized fractal dimension, D_q, dependence on q and SEM image size for PS/ HDPE 80/20 non-compatibilized (left) and compatibilized blends by 5 phr of SEBS (right).

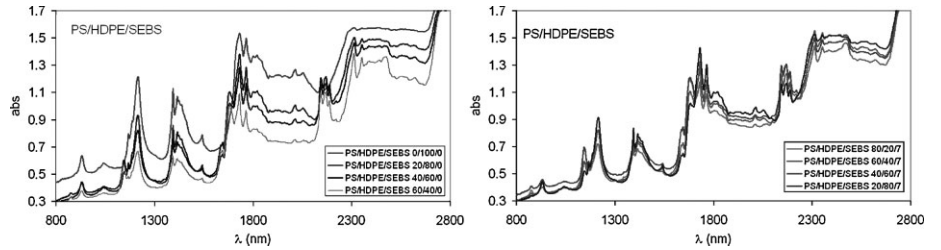

Figure 8.
NIR spectra of non-compatibilized (left) and compatibilized by 7 phr of SEBS (right) PS/HDPE blends.

spectra of PS and HDPE.[41] The 2D asynchronous correlation analysis reveals many out-of-phase band variations showing opposite trends in non-compatibilized and compatibilized blends. It is concluded from the asynchronous spectra that not only the phenyl rings of PS but also the CH_2 groups of HDPE play important roles in the formation of the blends.

Ratio of asynchronous and synchronous 2D correlation NIR spectra maps (proportional to tan θ) of non-compatibilized PS/HDPE blend is ''rougher'' than that of compatibilized PS/HDPE/ 7 phr SEBS blend (Figure 9). Two ''blend bands'' are identified at 1200 nm (HDPE) and 1452 nm (PS), whose origin has been attributed to the molecular level changes induced by the formation of blends. It is found that the NIR region of 1300-1560 nm is most suitable for 2D analysis of the specific interaction between PS and HDPE, while the region of 1800-800 nm is best for 2D analysis of the conformational features

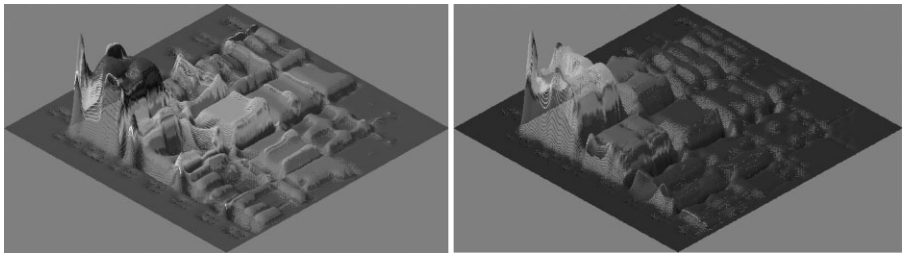

Figure 9.
Ratio of asynchronous and synchronous 2D correlation NIR spectra maps (proportional to tan θ, non-averaged, counts = 8) of non-compatibilized PS/HDPE/0 phr SEBS blend (left), and compatibilized PS/HDPE/ 7 phr SEBS blend (right).

common to both components, and the region of 2100-2300 nm is best for conformational features unique to set PS/ HDPE. Near-infrared spectra have been described by the Hurst index H_{NIR} (Table 4). The H_{NIR} is correlated with the HDPE content of PS/ HDPE/ SEBS blends ($|R| = 0.645$; $F_{signif}(1,10) = 0.023$):

$$\text{Hurst index } H_{NIR} = 0.993 - 5.926 \times 10^{-5} \times \text{HDPE}\,(\%)$$

The Hurst index is around 0.99 at HDPE contents lower than 60%, and then it starts to fall-off at HDPE content higher than 60% in the PS/HDPE/SEBS blends.

Mechanical Properties

As the content of HDPE in PS/HDPE blends increases the following changes are visible: the tensile strength decreases, while the elongation at break and room temperature notched Izod impact strength (NIRT) increase. Those changes are more expressed in the blends with SEBS as compatibilizer and increase with content of SEBS. The increasing of elongation at break and impact strength is particularly visible in blend with HDPE as continuous phase. It is in agreement with the morphological structure of PS/ HDPE/ SEBS blends and DMA measurements, which indicate the improvement of the compatibility.[42,43] The decreasing of tensile strength with the addition of SEBS is not such pronounced as increasing of elongation at break and notched Izod impact strength, what is important for the use PS/ HDPE/ SEBS blends in construction. Phase inversion[44] can be observed as the step change in the elongation at break. Addition of SEBS as an interfacial modifier result in a shift of the percolation threshold for

Table 4.
Hurst index of near-infrared spectra H_{NIR} determined by (R/S) method.

PS (phr)	HDPE (phr)	SEBS (phr)	Hurst index H_{NIR}	St. dev. H_{NIR}	R^2
0	100	0	0.9842	0.0013	0.9965
20	80	5	0.9895	0.0010	0.9975
20	80	7	0.9889	0.0010	0.9975
40	60	0	0.9913	0.0010	0.9976
40	60	5	0.9906	0.0010	0.9976
40	60	7	0.9916	0.0010	0.9977
60	40	0	0.9897	0.0010	0.9979
60	40	5	0.9923	0.0010	0.9978
60	40	7	0.9924	0.0010	0.9978
80	20	5	0.9895	0.0011	0.9978
80	20	7	0.9899	0.0010	0.9978
20	80	0	0.9871	0.0010	0.9976

dispersed PS to higher concentrations. The region of phase inversion is shifted from 22.5% wt. PS (for non-compatibilized blends PS/ HDPE) to 37% wt. PS (for compatibilized blends with 5 and 7 phr SEBS). The shift in the percolation threshold to higher values is related to lower elongation of the PS dispersed phase after interfacial compatibilization. These results indicate that an interfacial modifier significantly influences percolation phenomena without shifting the region of phase inversion. The impact of blends morphology on mechanical properties is judged by the correlation of mechanical properties with the fractal indices. So, the elongation at break e_b is best described by the fractal indices from thinned SEM images $D_{WBW,ZS}$ (from thinned SEM images of 198.8 μm^2 size) by a linear function($|R| = 0.910$; $F_{signif}(1,4) = 0.011$):

$$e_b\,(\%) = -122.8 + 74.18 \times D_{WBW,ZS}$$

The thinning has produced mesh like images that remind of a mesh like network contributing to the mechanical properties, especially the elongation at break. Tensile strength can be described by a statistically significant linear function of the box counting fractal index D_{WBW} (from SEM images of 198.8 μm^2 size, $|R| = 0.830$; $F_{signif}(1,4) = 0.040$):

$$\text{Tensile strength (MPa)} = 67.81 - 23.88 \times D_{WBW}$$

Similar linear function can be used to describe the notched impact strength at room temperature (NIRT), also, as a function of the box counting fractal index D_{WBW} (from SEM images of 198.8 μm^2 size, $|R| = 0.811$; $F_{signif}(1,4) = 0.049$):

$$\text{NIRT}\,(kJ/m^2) = -16.13 + 9.432 \times D_{WBW}.$$

The impact of blends morphology on mechanical properties is confirmed by the correlation of mechanical properties with the fractal indices. The varying fractal morphology and its effect on properties suggest that fractal induced morphology change can likely enhance mechanical performance in immiscible polymer blends. A fundamental question on the applicability of fractal analysis to fractured blend surfaces is if surfaces are genuine self-similar objects. Results presented to here show that blends specimen broken surfaces are not truly fractal because they do not show the highly hierarchical structure characteristic of the artificial fractal objects. Nevertheless, the fractal analysis gives an effective dimension that can be used to measure the complexity of highly complex structures such as fractured surfaces. Consequently, this study emphasizes the usefulness of fractal analysis in studying polymer blends.

A Survey of Results

The correlation between the composition of PS/HDPE/SEBS blends, morphological structure, mechanical properties, creep resistance and rheological properties are obtained. It is established that all examined properties depend on the content of HDPE and presence of SEBS block copolymer, which acts as a compatibilizer. It is evident to SEM analysis and examined properties, notched impact strength (NIRT), elongation at break and creep/ recovery values were increased in PS/HDPE/SEBS blends, while the process parameters, storage modulus and creep modulus are decreased with HDPE content. The PS/HDPE blend morphology varies drastically around its co-continuous composition and is a prominent function of the SEBS compatibilizer content. This variation has been explained in terms of break-up and coalescence of polymer pellets, which is a strong function of SEBS compatibilizer content. The SEBS compatibilizer content limits the kinetics of polymer droplet breakdown and dispersion. This effect is reflected the morphology of the blends produced under the constant processing conditions. The increase in domain size of PS as SEBS compatibilizer content decreases from zero is a result of induced coalescence during the long residence times and exposed to the low shear rates present under these conditions. SEM

observations of PS/HDPE/SEBS blends reveal more homogeny morphology and the presence of new layer in the blend with higher SEBS content and HDPE as continuous phase what suggest better adhesion. It is in agreement with the higher impact strength, elongation at break and creep values of compatibilized blends and their increasing with higher SEBS content. However, the compositional variations do not necessarily improve the mechanical properties of blends because the most efficient morphology might not be obtained at any composition if fixed extruder processing parameters are used. Generally, polymer blends comprising crystallizable components exhibit complex morphologies due to the competition of the micro-phase separation and crystallization of each blend component. The present creation of the fractal micro-domain structures from the crystallizable polymer blend components is attributed to the crystallization mediated segregation and organization for which the initial form can provide a seed of fractal molecular organization.

Conclusion

In this paper, we proposed fractal approaches for correlating polymer blends processing and morphology. The evidence is compelling that morphological fractals are connected to the processing randomness.

Acknowledgements: This work has been financially supported by Ministry of Science, Education and Sport of Croatia (Project no. 125-125 2971-2578). We appreciate technical help from M. Tudja, Ph. D. (PLIVA Ltd, Zagreb, Croatia).

[1] T. Y. Kim, D. M. Kim, W. J. Kim, T. H. Lee, K. S. Suh, *J. Poly. Sci., Part B* **2004**, *42*, 2813.
[2] L. A. Utracki, "*Comemercial Polymer Blends*", Chapman and Hall, London 1998.
[3] B. Xu, J. Simonsen, W. E. Rocheford, *J. Appl. Poly. Sci.* **2000**, *76*, 1100.
[4] B. A. Hegberg, G. R. Brenniman, W. H. Hallenback, "*Mixed Plastics Recylicling Technology*", Noyes Data Corp., Park Ridge, NJ 1992.
[5] L. Y. Yang, D. Bigio, T. G. Smith, *J. Appl. Poly. Sci.* **1995**, *58*, 129.
[6] C. P. Park, G. P. Clingerman, *Plast Eng.* **1997**, *53*, 97.
[7] V. Rek, T. Holjevac Grguric, Z. Jelcic, *Macromol. Symp.* **1999**, *148*, 425.
[8] V. Rek, T. Holjevac Grguric, Z. Jelcic, *Macromol. Symp.* **2003**, *202*, 127.
[9] H. E. Hurst, *Trans. Am. Soc. Civil Eng.* **1951**, *116*, 770–880.
[10] M. S. Taqqu, V. Teverovsky, W. Willinger, *Fractals* **1995**, *3*, 785.
[11] T. Karagiannis, M. Faloutsos, M. Molle, *Computer Communication Review* **2003**, *33*, 81–93.
[12] P. Abry, D. Veitch, *IEEE Transactions on Information Theory*, **1998**, *44*, 2–15.
[13] B. B. Mandelbrot, J. R. Wallis, *Water Res. Res.* **1969**, *5*, 228–267.
[14] Z. Jelcic, T. Holjevac-Grguric, V. Rek, *Polym. Deg. Stab.* **2005**, *90*, 295–302.
[15] B. B. Mandelbrot, "*The Fractal Geometry of Nature*", W.H. Freeman& Co., New York 1983.
[16] A. H. Barrett, M. Peleg, *Lebensm. Wiss. Technol.* **1995**, *28*, 553–563.
[17] T. Nagai, T. Yano, *J. Food Sci.* **1990**, *55*, 1334–1337.
[18] A. Calzetta-Resio, R. J. Aguerre, C. Suarez, *J. Food Eng.* **1999**, *42*, 51–57.
[19] A. G. Marangoni, D. Rousseau, *JAOCS* **1996**, *73*, 991–994.
[20] P. Podsiadlo, G. W. Stachowiak, *Wear* **1999**, *230*, 184–193.
[21] C. L. Jones, "Image Analysis of Fungal Biostructure by Fractal and Wavelet Techniques", Thesis, 1998.
[22] A. D. Fowler, H. E. Stanley, G. Daccord, *Nature*, **1989**, *341*, 134–138.
[23] D. Bérubé, M. Jébrak, *Computers and Geosciences* **1999**, *25*, 1059–1071.
[24] P. Gwaze, O. Schmid, H. J. Annegarn, M. O. Andreae, J. Huth, G. Helas, *J. Aerosol Sci.* **2006**, *37*, 820–838.
[25] P. Meakin, B. Donn, G. W. Mulholland, *Langmuir*, **1989**, *5*, 510–518.
[26] T. Higuchi, *Physica D* **1988**, *31*, 277–283.
[27] H. Ahammer, T. T. J. DeVaney, *Chaos.* **2004**, *14*, 183–188.
[28] G. Chinga, Ø. Gregersen, B. Dougherty, *J. Micros. Anal.* **2003**, *84*, 5–7.
[29] T. Y. Zhang, C. Y. Suen, *Commun. ACM* **1984**, *27*, 236–239.
[30] I. Noda, Y. Ozaki, "*Two-dimensional Correlation Spectroscopy – Applications in Vibrational and Optical Spectroscopy*", Wiley, Chichester 2004.
[31] I. Noda, *Appl. Spectrosc.* **1990**, *44*, 550.
[32] I. Noda, *Appl. Spectrosc.* **1993**, *47*, 1329.

[33] P. J. Tandler, P. de. B. Harrington, H. Richardson, *Anal. Chim. Acta* **1998**, *368*, 45–57.
[34] T. Nishioka, Y. Ren, N. Tsubahara, K. Nakashima, I. Noda, Y. Ozaki, *Anal. Sci.* **2001**, *17*, i689.
[35] Y. Ren, T. Murakami, T. Nishioka, K. Nakashima, I. Noda, Y. Ozaki, *Macromolecules* **1999**, *32*, 6307–6318.
[36] S.-W. Kuo, C.-F. Huang, P.-H. Tung, W.-J. Huang, J.-M. Huang, F.-C. Chang, *Polymer* **2005**, *46*, 9348.
[37] C.-F. Huang, S.-W. Kuo, F.-J. Lin, W.-J. Huang, C.-F. Wang, W.-Y. Chen, F.-C. Chang, *Macromolecules* **2006**, *39*, 300.
[38] J. Li, B. D. Favis, *Polymer* **2001**, *42*, 5047–5053.
[39] W. Brostow, H. E. Hagg Lobland, M. Narkis, *J. Mater. Res.* **2006**, *21*, 2422.
[40] T. Kallel, V. Massardier Nageotte, M. Jaziri, J. F. Gerard, B. Elleuch, *J. Appl. Poly. Sci.* **2003**, *90*, 2475.
[41] D. A. Burns, E. W. Ciurczak, *Handbook of Near-infrared Analysis*, Edition 3rd, CRC Press, **2007**, *535*, 539–540.
[42] T. Li, V. A. Topolkaraev, E. Baer, X. Z. Ji, R. P. Quirk, *J. Poly. Sci. Polym. Phys.* **1995**, *33*, 667.
[43] C. P. Park, G. P. Clingerman, *Plast. Eng.* **1997**, *53*, 97.
[44] D. Bourry, B. D. Favis, *J. Polym. Sci., Polym. Phys. Ed.* **1998**, *36*, 1889–1899.

